ELSEVIER

Materials Chemistry and Physics 71 (2001) 40–46

MATERIALS CHEMISTRY AND PHYSICS

www.elsevier.com/locate/matchemphys

Cathodic electrodeposition and analysis of SnS films for photoelectrochemical cells

B. Subramanian [a], C. Sanjeeviraja [a,*], M. Jayachandran [b]

[a] *Department of Physics, Alagappa University, Karaikudi 630 003, India*
[b] *Central Electrochemical Research Institute, Karaikudi 630 006, India*

Received 13 April 2000; received in revised form 22 August 2000; accepted 30 October 2000

Abstract

Thin films of p-SnS were cathodically electrodeposited on tin oxide conducting glass substrates from aqueous solution containing $SnCl_2$ and $Na_2S_2O_3$. The mechanism of electrochemical co-deposition of tin and sulphur is investigated by cyclic voltammetry. Deposits have been characterised with X-ray diffractograms, microstructure analysis, chemical analysis, optical and electrical measurements. The films were found to be polycrystalline with an optical energy gap of 1.15 eV. Mott–Schottky plot has been drawn (in the dark condition) to evaluate the semiconductor parameters. A photoelectrochemical cell with the configuration of p-SnS|Fe^{3+}, Fe^{2+}|Pt yielded a short-circuit current density of 0.65 mA cm^{-2}, an open-circuit voltage of 320 mV under 100 mW cm^{-2} illumination.

Keywords: Cathodic electrodeposition; Photoelectrochemical cells; Tin sulfide; Thin films

1. Introduction

Interest in the use of photoelectrochemical (PEC) solar cells for low-cost energy conversion has led to an extensive research in the search for thin film polycrystalline materials [1,2]. Tin sulfide is a layered semiconductor compound which is a promising candidate in the field of photoelectrochemical solar energy conversion due to its highly stable nature. It is basically the combination of tin, an element from group IV and S the member of group VI. In layered type chalcogenides, within each layer, the atoms are predominantly bound together by covalent forces. The bonds between the layers are extremely week due to Van der Waals forces [3]. SnS has orthorhombic structure which is psuedotetragonal and may be thought of as a rather strongly distorted sodium chloride structure. The crystal consists of double layers perpendicular to the *c*-axis in which the Sn and S atoms are tightly bound. The bonding between these layers is much weaker as shown by larger interatomic distances and by a (0 0 1) cleavage plane [4].

The usage of SnS in photovoltaic/PEC solar cells has attracted much interest, since its optical bandgap of 1.08 eV is similar to that of silicon [5]. The effect of bath parameters on the thickness of the chemically deposited SnS films has been reported [6]. Nair and Nair [7] have reported the chemical bath deposition of Cu_xS and SnS thin films on glass substrates and illustrated their applications in solar control coatings. Mishra et al. [8] have carried out electron probe microanalysis and X-ray photoelectron spectroscopy studies for electrodeposited SnS films. PEC behavior of SnS pellet was studied by Sharon et al. [9] and has reported a conversion efficiency of 0.63%.

In this paper, we report the cathodic electrodeposition for the synthesis of SnS thin films which is more attractive since it offers the advantages of economy, convenience and several experimental parameters can be controlled more precisely. A detailed account of the electrochemistry involved in the deposition of Sn, S and Sn + S is presented. The materials properties and the results on the photoelectrochemical cell performance are reported.

2. Experimental

2.1. Preparation and characterisation of SnS films

The deposition bath contains 5 mM of $SnCl_2$, 2.5 mM of $Na_2S_2O_3$, and the pH of the solution was adjusted to 1.5. Films were deposited using a three electrode cells with water circulation. An EG&G-PAR model 362 scanning potentiostat/galvanostat with *x–y–t* recorder was employed

* Corresponding author. Fax: +91-4565-35202.
E-mail address: alagappa@md3.vsnl.net.in (C. Sanjeeviraja).

0254-0584/01/$ – see front matter
PII: S0254-0584(00)00526-5

for recording the cyclic voltammograms (CV) and controlling the deposition potentials. Tin oxide (TO) coated glass substrates were rinsed well with deionized water and used as cathode for all depositions. The deposition area was kept constant as 1 cm^2. A platinum electrode served as the anode and a saturated calomel electrode (SCE) was employed as the reference electrode unless otherwise stated, all the potentials are expressed with respect to SCE. The bath temperature was varied between 28 and 75°C using a constant temperature bath. Annealing of films was carried out in vacuum at 250°C for 30 min. X-ray diffractometry with Cu Kα radiation was performed on JEOL JDX 803a diffractometer. The scanning electron microscopic (SEM) study was carried out using JSM 6400 JEOL scanning electron microscope. AFM analysis was characterised by Nanoscope® E scanning probe microscopy 3138J. The X-ray photoelectron spectroscopy (XPS) spectrum was taken using VG MKII ESCA spectrometer. The transmission and absorption spectra were taken using a double beam Hitachi UV–VIS–NIR U3400 spectrophotometer in the wavelength region of 400–1200 nm with a blank tin oxide coated glass substrate kept in the reference channel.

2.2. Fabrication of photoelectrochemical solar cells

A three electrode configuration was used for all photoelectrochemical measurements. The counter electrode was platinum, the reference electrode was a SCE placed very near to the p-SnS thin film photoelectrode during the measurement of cell output. The distance between the semiconductor photoelectrode and counter electrode was kept constant at 1.0 cm. The redox electrolyte, (aq) 0.1 M $FeCl_3/FeCl_2$ (0.05 M H_2SO_4), was prepared using analytical reagent (AR) grade chemicals. SUNLUX 500 W/250 V tungsten filament-halogen lamp was used for illuminating the electrode with a light intensity of 100 mW cm^{-2}. The illumination intensity was measured by CEL suryamapi instrument. A Vasavi LCR bridge with an in-built function generator at a frequency of 1 kHz was used for the measurement of space-charge capacitance to obtain Mott–Schottky plot.

3. Results and discussion

3.1. Electrochemistry of Sn and S

The individual electrochemical reaction steps involved in the deposition of Sn and S are given as follows:

1. Sn reduction: it involves a two electron transfer reaction

$$\mathrm{Sn^{2+} + 2e^- \leftrightarrow Sn(s)} = E^0\left(\frac{\mathrm{Sn^{2+}}}{\mathrm{Sn}}\right) + \left(\frac{RT}{2F}\right)\ln\frac{a_{\mathrm{Sn^{2+}}}}{a_{\mathrm{Sn}}} = -0.38V_{\mathrm{SCE}} + 0.0295\log\frac{a_{\mathrm{Sn^{2+}}}}{a_{\mathrm{Sn}}}$$

2. S reduction

$$\mathrm{S_2O_3^{2-} + 6H^- + 4e^- \leftrightarrow 2S(s) + 3H_2O} = E^0\left(\frac{\mathrm{S^{2+}}}{\mathrm{S}}\right) + \left(\frac{RT}{4F}\right)\ln\left(\frac{a_{\mathrm{S_2O_3^{2-}}}}{a_{\mathrm{S}}}\right) + \left(\frac{3RT}{6F}\right)\ln\mathrm{OH^+} = +0.26V_{\mathrm{SCE}} + 0.0148$$

Here, E^0 are the equilibrium electrode potentials expressed with reference to SCE; 'a' is the activity of respective ions in the bulk solution and the deposit ($a = 1$, for an ion in the solid deposit); and OH^+ is the concentration of hydrogen ions. Sn(s) and S(s) are respective species in the solid deposit.

For simultaneous co-deposition of Sn and S, the concentration and pH of the electrolyte should be adjusted so that the electrode potentials of the individual species come closer to each other. The pH of the bath was fixed at 1.5 at which condition the disproportionation of $S_2O_3^{2-}$ takes place to release S^{2-} for the formation of SnS compound on the cathode [10].

3.2. Electrodeposition of Sn, S and SnS films

To obtain co-deposited SnS films and in the control of film stoichiometry, the concentration of Sn and S plays a major role. A Sn(II) to S(II) ion ratio of about 0.5 is found favourable to maintain the bath without any precipitation. The deposition potential was fixed through cyclic voltammetry experiments in aqueous solutions of tin and thiosulphate ions. Initially voltammograms of $SnCl_2$ and $Na_2S_2O_3$ are recorded. To study the formation of binary compounds, the voltammograms were obtained for the solution containing the mixtures of $SnCl_2$ and $Na_2S_2O_3$. The solution was continuously stirred using a magnetic stirrer and left to attain steady-state. Purified N_2 gas was purged into the electrolyte solution for at least 5 min to remove the dissolved oxygen before starting the experiment.

The cyclic voltammogram obtained in aqueous solution of 5.0 mM of Sn (II) on TO coated glass electrode is shown in Fig. 1(a). The forward scan current remains at a very low value upto −0.4 V. The current starts increasing afterwards and a cathodic peak is observed at about −0.72 V. This cathodic current flow is associated with Sn (II) reduction process. The reverse scan forms a loop like curve confirming the formation of tin film all over the cathodic surface. This reverse scan crosses the forward scan at −0.49 V. The anodic peak is observed at −0.42 V. This well defined anodic peak confirms the complete dissolution of the tin layer deposited during the cathodic scan. The reversible nature of the tin deposition mechanism is confirmed by the nearly constant potential values of the anodic peaks recorded with different scan rates of 10, 20 and 100 mV s^{-1} [11].

The voltammogram obtained in the potential range of 0.0 to −1.0 V using a TO coated glass electrode in 2.5 mM $Na_2S_2O_3$ solution is shown in Fig. 1b. The cathodic current starts flowing at about −0.63 V. A shoulder at −0.7 V may

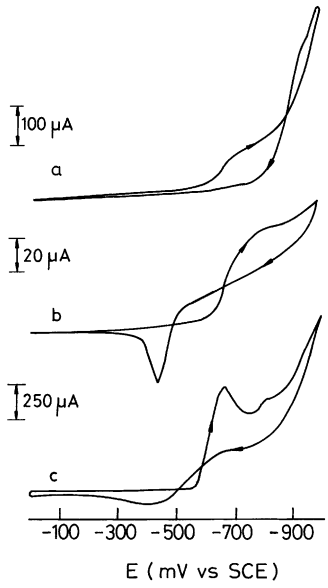

Fig. 1. Cyclic voltammogram of (a) 2.5 mM $Na_2S_2O_3$; (b) 5 mM $SnCl_2$; (c) 5 mM $SnCl_2$ + 2.5 mM $Na_2S_2O_3$. The scan rates were 20 mV/s.

be associated with the reduction of thiosulphate ions. This reduction wave may be due to the $S_2O_3^{2-}$ ions released during the disproportionation of $Na_2S_2O_3$ at the pH of 1.5. No significant change in the voltammograms is observed when scanning was performed at different rates. It is essential to analyse the interaction between tin and sulfur ion species as it provides the mechanism underlying the process of SnS formation. When 10 mM $S_2O_3^{2-}$ ions were added to the Sn(II) solution some marked changes are observed in the voltammetric curves as shown in Fig. 1(c). The cathodic current onset was shifted to −0.57 V followed by a clear cathodic peak at −0.67 V and a broader peak at about −0.8 V. The presence of thiosulphate ions increased the over potential for the reduction of Sn(II) ions which may be due to the complex formation ability of $S_2O_3^{2-}$ ions with Sn(II) ions. These two peaks might have been associated with the reduction of Sn(II) and $S_2O_3^{2-}$ ions leading to their co-deposition.

A relatively smaller and broader stripping peak is observed at about −0.4 V. It confirms the formation of a stable tin compound during the cathodic scan. The presence of $S_2O_3^{2-}$ ions dictates the deposition process and the formation of SnS film. Further, the observed increase in cathodic peak height and the reduced anodic peak height with repeated scanning confirms the formation of stable SnS films at pH 1.5. When scan rate is increased, the cathodic peak slightly shifts towards the positive potentials. As the scan rate increases the stripping peak height reduces which again indicates the formation of tin rich deposit at low scan rates.

3.3. Structural and microstructural characterisation of SnS films

Fig. 2(a) shows the typical X-ray diffractogram of the as-prepared SnS films and Table 1 compares the d values

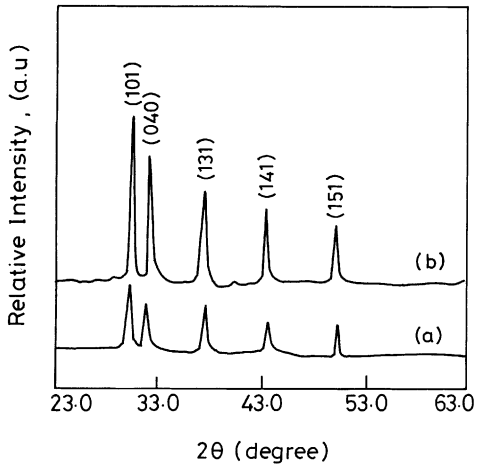

Fig. 2. X-ray diffraction pattern of SnS film (a) as-deposited film; (b) vacuum annealed film.

Table 1
Comparison of d values of p-SnS with standard ASTM data

Sl. no.	$d_{observed}$ (Å)	d_{ASTM} (Å)	h	k	l
1	2.910	2.931	1	0	1
2	2.769	2.797	0	4	0
3	2.384	2.305	1	3	1
4	2.030	2.024	1	4	1
5	1.763	1.779	1	5	1

calculated from X-ray diffractogram with the standard ASTM values. It is found that there is a fair agreement in d values. Fig. 2(b) indicates the XRD pattern of the annealed SnS film at 250°C for 30 min in vacuum. The diffractograms indicate the polycrystalline nature of the film with all peaks corresponding to the orthorhombic structure with lattice constants $a = 0.403$ nm, $b = 1.145$ nm and $c = 0.399$ nm. They compare well with the reported values [8]. Annealing at 250°C improves the crystallinity. Fig. 3 shows the scanning electron micrograph of the as-grown SnS thin film,

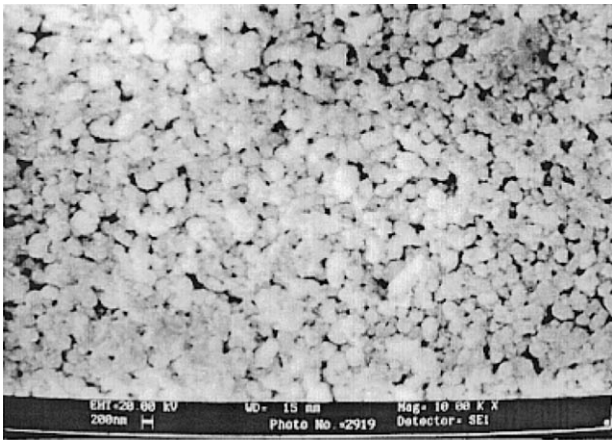

Fig. 3. A typical scanning electron micrograph of a thin film of p-SnS showing the microstructure.

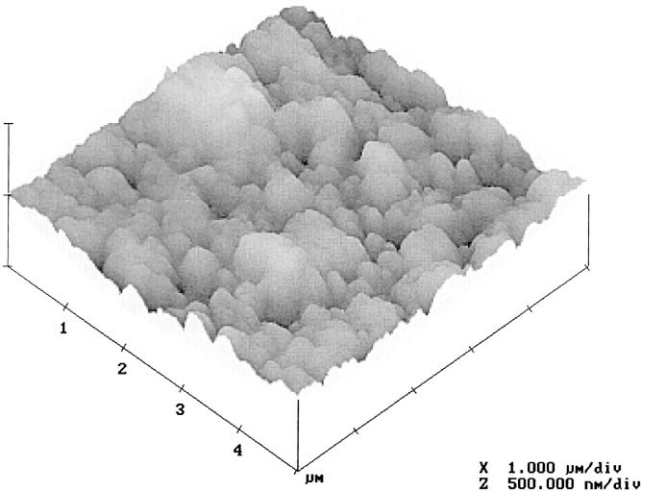

Fig. 4. AFM image of the surface of SnS film.

revealing the microstructure. The average size of the microcrystallites was determined by Cottrell's method [12] from SEM picture. It was found to be ≈580 nm. Grain size of the electrode film is important as it governs the shunt resistance R_{sh}, which is one of the parameters governing the efficiency of the PEC cell. Annealing of the films improved the surface smoothness and no pinholes were observed as evident from the SEM analysis. The grain size also increased to about 760 nm, leading to coalescence of the grains.

The surface smoothness of the SnS films prepared by electrodeposition was further characterized by AFM. Advantage of AFM is its capacity to probe the minute details related to the individual grains and inter-grain regions as well in three-dimensional form. Fig. 4 shows the three-dimensional representation of a 5 μm × 5 μm area of the as-deposited SnS film. The thickness of the film is about 1.0 μm. The average grain size determined using standard statistical averaging technique is about 540 nm. AFM picture shows the presence of high hills on top of a homogeneous granular background surface. The height of the hills is found increased as the thickness of the SnS film increases. This observation reveals that the growth of SnS film on TO substrates by electrodeposition is associated with the formation of three-dimensional grains in the perpendicular direction without lateral diffusion of ad-atoms on the surface parallel to the substrate. This may be attributed to the preferentially oriented crystalline nature of the TO substrate over which SnS film is deposited.

3.4. XPS studies

Fig. 5 contains a survey XPS spectrum of an electrodeposited p-SnS sample. The presence of the Sn and S on the gray-brown sample is confirmed from XPS spectrum. The presence of O and C are also evident on different samples. Quantitative analysis of these elements shows a surface atomic concentration of 40.1% for Sn, 37.5% for S, 8.5% for C and 13.9% for O. The significant level of O may be due to incipient corrosion process during the synthesis of films [13]. XPS data unequivocally rule out the presence of any SnS_2 or Sn_2S_3 in our SnS samples. After 2 + 2 min sputtering with argon ion, the atomic concentration is changed to 43.2% for Sn and 40.6% for S, which confirms the nearly stoichiometric, or slightly Sn-rich film. High-resolution analysis of the Sn and S binding energy peaks were performed. The Sn 3d 5/2 (485.5 eV) and 3/2 (494.1 eV) doublets were deconvoluted into contribution from a low binding energy component due to Sn in SnS. This is consistent with values reported for stoichiometric SnS deposits [14]. The S 2p 3/2 line is change corrected using C 1s line and energy 161.3 eV is similar to the reported values [8].

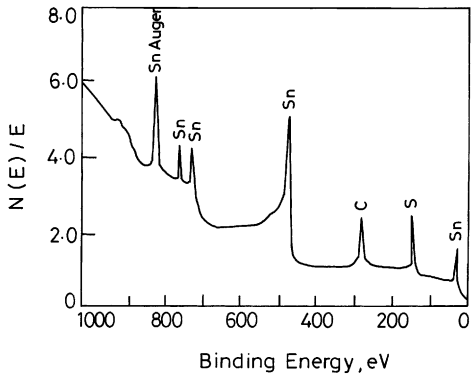

Fig. 5. Survey XPS spectrum for a SnS film after 2 + 2 min argon sputtering.

3.5. Optical properties

Fig. 6 shows representative plots of the optical absorbance and transmittance spectra obtained for the as-grown and annealed SnS deposit on tin oxide coated glass substrates in the region of 400–1400 nm. A pronounced absorption edge is evident in the vicinity of 750–800 nm for all samples. Since the plots of $(\alpha h\nu)^{1/2}$ versus $h\nu$ are linear, the indirect nature of the optical transition is observed. From the intercepts of the extrapolated linear region with $h\nu$ axis, a band

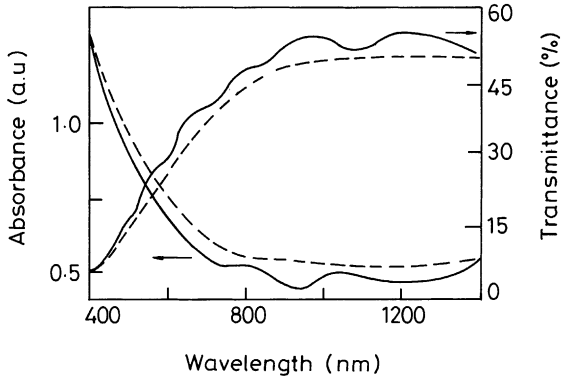

Fig. 6. Absorption and transmission spectra of SnS film — annealed film; --- as-deposited film.

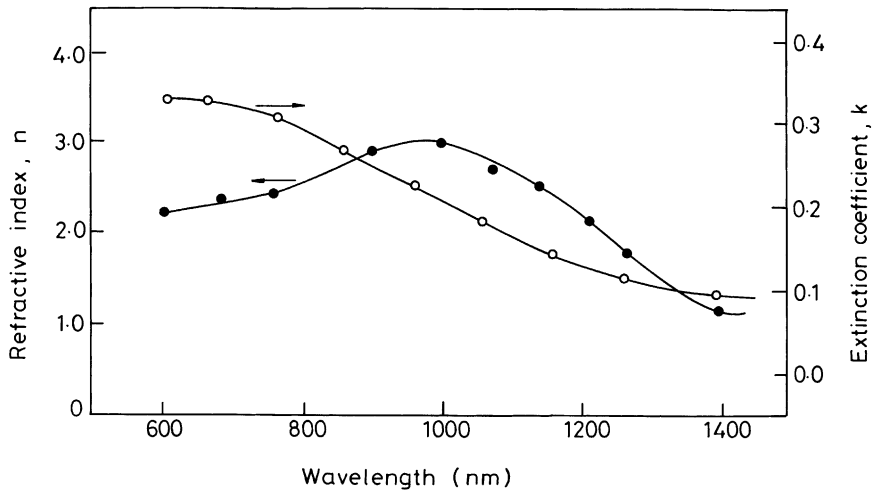

Fig. 7. Variation of n and k with wavelength for a SnS film.

gap value of 1.15 eV is observed. It is in good agreement with the reported values for SnS films [15]. The absorption coefficient for these films, near the fundamental absorption edge is larger than $2 \times 10^4\ \mathrm{cm}^{-1}$ which makes the SnS film as a suitable for solar cell fabrication. Annealing the films in vacuum at 250°C for 30 min increases the absorption behavior. The average thickness of the synthesized films have been calculated from the successive maxima of the interference pattern observed in the transmittance curves as 0.9 μm. The value is in agreement with 0.84 μm obtained from gravimetric method. The continuous differential descent (CDD) method [16] has been used to determine the optical constants, the refractive index (n) and extinction coefficient (k). Fig. 7 shows a maximum refractive index value of 2.9 at a wavelength of 1000 nm which corresponds to the band gap of the material. On either side of this wavelength the refractive index is decreased. The extinction coefficient for the films has been observed in the range of 0.1–0.3.

3.6. Electrical properties

Using the hot-probe method, it was observed that the as-deposited and the annealed films had p-type conductivity. The resistivity of the SnS films was measured by the van der Pauw method. The SnS film exhibited a resistivity of about 20 Ω cm. The current–voltage characteristics of the SnS films were linear when electrodes were prepared using silver paint, indicating that silver paint forms an ohmic contact to these films. Fig. 8 shows the variation in the dark conductivity with temperature from 300–450 K for the electrodeposited SnS film. The activation energy for the conduction was about 0.34–0.45 eV, suggesting the presence of deep acceptor levels in accordance with the results in the literature [15]. The vacuum annealed films showed a better conductivity with activation energy of about ~0.58 eV.

3.7. Characterisation of p-SnS|Fe^{3+}, Fe^{2+}|Pt PEC solar cells

3.7.1. Capacitance measurements

Fig. 9 shows the typical Mott–Schottky plot drawn using the capacitance data at a frequency of 1 kHz (in the dark) for the system p-SnS|Fe^{3+}, Fe^{2+}|Pt. The value of flat band potential was obtained using the following relation [17]

$$\frac{1}{C_{SC}^2} = \left(V - V_{fb} - \frac{k_B T}{e}\right) \frac{2}{\epsilon_0 \epsilon_s N_A e} \tag{1}$$

where ϵ_0 is the permittivity of free space, ϵ_s the permittivity of the semiconductor electrode, e the charge on the carriers, N_A the acceptor concentration, T the temperature of operation ≈ 300 K, k_B the Boltzmann's constant, and C_{SC} is the space charge capacitance. The negative slope of

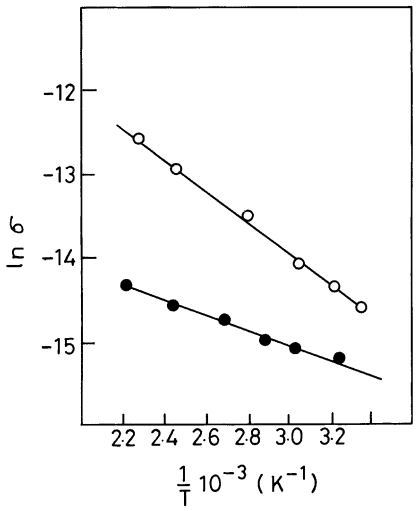

Fig. 8. Conductivity ($\ln \sigma$) vs. T^{-1} (10^3) for (a) as-deposited; (b) annealed SnS film.

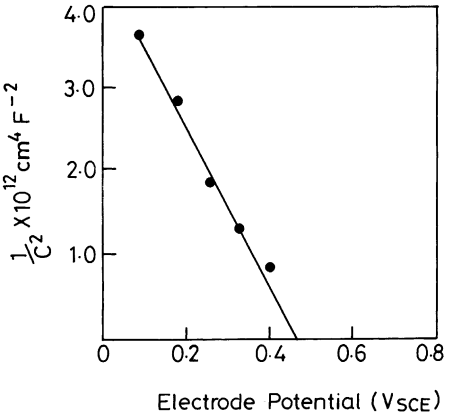

Fig. 9. Mott–Schottky plot for the p-SnS |Fe^{3+}, Fe^{2+}|Pt system at a frequency of 1 kHz.

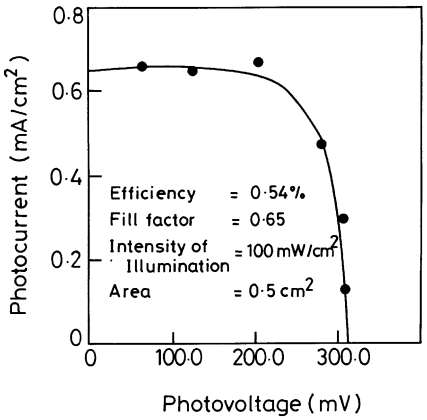

Fig. 10. Power output characteristics of p-SnS |Fe^{3+}, Fe^{2+}|Pt PEC cell.

the Mott–Schottky plot confirms the p-type conductivity of the SnS films. The intercept of the linear plot ($1/C^2 = 0$) was taken as the electrode potential of the semiconductor at which the band bending is zero. This potential is the flat — band potential and is equal to 0.46 V. The depletion layer width (w) was calculated from the equation

$$w = \left[\frac{2\epsilon_0\epsilon_s V_b}{eN_A}\right] \quad (2)$$

where V_b is the built-in voltage or the band bending. The semiconductor materials parameters of the SnS thin films obtained from the plot are given in Table 2.

3.7.2. Power output characteristics

Fig. 10 shows the power output characteristics of the PEC cell using vacuum annealed p-SnS films. The open circuit voltage was found to be, $V_{oc} = 320$ mV and the short circuit density was found to be, $J_{sc} = 0.65\,mA\,cm^{-2}$. The efficiency was 0.54% and the fill factor was 0.65. The low efficiency may be attributed to the low shunt resistance $R_{sh} = 2.5\,k\Omega$ because of the presence of grain boundaries in polycrystalline films which tend to be parallel to the film normal [17]. AFM picture shows the growth of the microcrystallites normal to the film plane, which provide the paths for leakage current. There is no leakage when the shunt resistance is infinite. The output of the PEC cell was constant for about 3 months. It means that SnS is stable chemically as well as photochemically and it should be an useful material for PEC solar cells.

Table 2
Semiconductor materials parameters obtained from Mott–Schottky plot of p-SnS thin film

Sl. no.	Physical parameter	Value obtained
1	Electrolyte used	Fe^{3+}/Fe^{2+}
2	Redox Fermi level of the electrolyte E_F	$0.53V_{SCE}$
3	Flat band potential V_{FB}	$0.46V_{SCE}$
4	Acceptor concentration, N_A	$7.36 \times 10^{16}\,cm^{-3}$
5	Density of states in the valance band, N_v	$4.13 \times 10^{19}\,cm^{-3}$
6	Built in voltage (band bending), V_b	0.07 V
7	Depletion width, w	4.2×10^{-5} cm
8	Carrier type	p

4. Conclusions

SnS films have been cathodically electrodeposited on tin oxide coated glass substrates from aqueous solution containing $SnCl_2$ and thiosulphate ions. A nearly stoichiometric SnS films, as evident from XPS studies, were prepared at a deposition potential of −800 mV, keeping the bath pH at 1.5 and maintaining the bath temperature at 65°C. The films are polycrystalline with orthorhombic structure and show p-type semiconducting nature. Annealing in vacuum at 250°C for 30 min showed improved crystallinity and increased grain size as observed from the SEM and XRD analyses. Optical measurements revealed the indirect nature of the films. A photoelectrochemical conversion efficiency of 0.54% is obtained for the system using p-SnS as photocathode.

Acknowledgements

The authors thank Dr. V. Ganesan, IUC for DAEF, Indore, India for his support to carry out AFM studies. Acknowledgements are also due to RSIC, IIT, Madras, Chennai, India for providing XPS facilities. Authors would acknowledge the AICTE, New Delhi, India for the financial support to carry out this work.

References

[1] S. Licht, Solar Energy Mater. Sol. Cell 38 (1995) 305.
[2] Z. Loizos, N. Syrellis, G. Maurin, Thin Solid Films 204 (1991) 139.
[3] F. Hulliger, Structural chemistry of layer type phases, in: F. Levy, D. Reidel (Eds.), Dordrecht-Holland/Boston, 1976.
[4] W. Albers, C. Haas, F. Van der Masesn, J. Phys. Chem. Solids 15 (1960) 306.

[5] M. Ristov, Gj. Sinadinovski, I. Groydanov, M. Mitreki, Fizika 21 (1989) 320.
[6] P. Pramanik, P.K. Basu, S. Biswas, This solid films 150 (1987) 267.
[7] M.T.S. Nair, P.K. Nair, Semicond. Sci. Technol. 6 (1991) 132.
[8] K. Mishra, K. Rajeshwar, A. Weiss, M. Murley, R.D. Engelken, M. Slayton, H.E. McCloud, J. Electrochem. Soc. 136 (1989) 1915.
[9] M. Sharon, P. Veluchamy, C. Natarajan, D. Kumar, Electrochim. Acta 36 (1991) 1107.
[10] M. Jayachandran, M.J. Chokalingam, V.K. Venkatesan, J. Mater. Sci. Lett. 8 (1989) 563.
[11] L. Peter, Electrochim. Acta 23 (1978) 165.
[12] A. Cottrell, Introduction to Metallurgy, Arnold, London, 1975, p. 173.
[13] Z. Zainal, M.Z. Hussein, A. Ghazali, Sol. Energy Mater. Sol. Cells 40 (1996) 347.
[14] R.B. Shalvoy, G.B. Fischer, P.J. Stiles, Phys. Rev. B 15 (1977) 1680.
[15] R.D. Engelken, H.E. McCloud, E. Lee, M. Slayton, H. Ghoreishi, J. Electrochem. Soc. 134 (1987) 2696.
[16] F.A. Bondar, Yu.A. Kulypin, Y.M. Poporich, Thin Solid Films 55 (1975) 255.
[17] V.D. Das, L. Damodare, Solid State Commun. 99 (1996) 723.